Molecular Therapy
Nucleic Acids
Original Article

Mutant Allele-Specific CRISPR Disruption in DYT1 Dystonia Fibroblasts Restores Cell Function

Lilian Cruz,[1,18] Bence György,[1,2,3,4,18,19] Pike See Cheah,[1,5] Benjamin P. Kleinstiver,[6,7,12] William A. Eimer,[1,8] Sara P. Garcia,[9] Nutan Sharma,[1] Laurie J. Ozelius,[1] D. Cristopher Bragg,[1] J. Keith Joung,[6,10,11,12] Osmar Norberto de Souza,[13,14] Luis Fernando Saraiva Macedo Timmers,[15,16] and Xandra O. Breakefield[1,17]

[1]Department of Neurology, Massachusetts General Hospital, Harvard Medical School, Boston, MA, USA; [2]Neurobiology Department, Harvard Medical School, Boston, MA, USA; [3]Institute of Molecular and Clinical Ophthalmology Basel, Basel, Switzerland; [4]Department of Ophthalmology, University of Basel, Basel, Switzerland; [5]Department of Human Anatomy, Faculty of Medicine and Health Sciences, Universiti Putra Malaysia, Serdang, Malaysia; [6]Department of Pathology, Massachusetts General Hospital, Harvard Medical School, Boston, MA, USA; [7]Center for Genomic Medicine, Massachusetts General Hospital, Boston, MA, USA; [8]Genetics and Aging Research Unit, MassGeneral Institute for Neurodegenerative Disease, Charlestown, MA, USA; [9]Molecular Pathology Unit, Massachusetts General Hospital, Charlestown, MA, USA; [10]Center for Cancer Research, Massachusetts General Hospital, Charlestown, MA, USA; [11]Center for Computational and Integrative Biology, Massachusetts General Hospital, Charlestown, MA, USA; [12]Department of Pathology, Harvard Medical School, Boston, MA, USA; [13]Laboratory for Bioinformatics, Modelling and Simulation of Biosystems-LABIO, Pontifical Catholic University of Rio Grande do Sul-PUCRS, Porto Alegre City, Brazil; [14]Graduate Program in Cellular and Molecular Biology (PPGBCM), PUCRS, Porto Alegre - RS, Brazil; [15]University of Taquari Valley-Univates, Lajeado City, Brazil; [16]Graduate Program in Biotechnology (PPGBiotec), Univates, Lajeado City, RS, Brazil; [17]Department of Radiology, Massachusetts General Hospital, Harvard Medical School, Boston, MA, USA

Most individuals affected with DYT1 dystonia have a heterozygous 3-bp deletion in the *TOR1A* gene (c.907_909delGAG). The mutation appears to act through a dominant-negative mechanism compromising normal torsinA function, and it is proposed that reducing mutant torsinA may normalize torsinA activity. In this study, we used an engineered Cas9 variant from *Streptococcus pyogenes* (SpCas9-VRQR) to target the mutation in the *TOR1A* gene in order to disrupt mutant torsinA in DYT1 patient fibroblasts. Selective targeting of the DYT1 allele was highly efficient with most common non-homologous end joining (NHEJ) edits, leading to a predicted premature stop codon with loss of the torsinA C terminus (delta 302–332 aa). Structural analysis predicted a functionally inactive status of this truncated torsinA due to the loss of residues associated with ATPase activity and binding to LULL1. Immunoblotting showed a reduction of the torsinA protein level in Cas9-edited DYT1 fibroblasts, and a functional assay using HSV infection indicated a phenotypic recovery toward that observed in control fibroblasts. These findings suggest that the selective disruption of the mutant *TOR1A* allele using CRISPR-Cas9 inactivates mutant torsinA, allowing the remaining wild-type torsinA to exert normal function.

INTRODUCTION

TorsinA was discovered as a novel 332-aa protein in which a specific 3-bp deletion (GAG) causing loss of a glutamate residue at position 303 underlies the early onset movement disorder DYT1 torsion dystonia.[1–3] TorsinA was predicted to be an AAA+ ATPase, and the first and only one localized within the contiguous lumen of the endoplasmic reticulum (ER) and nuclear envelope (NE).[1,4–6] In the ER, torsinA is associated with protein quality control,[7–9] redox sensing,[10] membrane homeostasis,[11] and lipid metabolism.[12,13] In the NE, functions encompass positioning of the nucleus during migration and morphology of the nuclear membrane,[14–16] biogenesis of nuclear pores,[17–19] and egress of large ribonucleoprotein particles and viral capsids out through the NE into the cytoplasm.[20,21] DYT1 patient fibroblasts showed a deficit in passage of newly replicated herpes simplex virus type 1 (HSV-1) capsids out of the nucleus into the cytoplasm as compared to control fibroblasts.[22]

TorsinA was initially predicted to have a hexameric structure[23,24] with several proposed models, including a torsinA homohexamer,[25] a 3:3 torsinA:LULL1 or LAP1 heterohexamer,[26] and a 1:1 torsin:LULL1 or LAP1 heterodimer/hexamer,[3] with the most recent studies favoring the homohexamer with LAP1 and LULL1 interactions triggering ATP

Received 6 April 2020; accepted 12 May 2020;
https://doi.org/10.1016/j.omtn.2020.05.009.

[18]These authors contributed equally to this work.

[19]Present address: Clinical Translation, Institute of Molecular and Clinical Ophthalmology Basel (IOB), Department of Ophthalmology, University of Basel, Mittlere Strasse 91, 4031 Basel, Switzerland

Correspondence: Xandra O. Breakefield, PhD, Department of Neurology, Massachusetts General Hospital, Harvard Medical School, 13th Street, Building 149, Charlestown, MA 02129, USA.
E-mail: breakefield@hms.harvard.edu
Correspondence: Bence György, MD, PhD, Clinical Translation, Institute of Molecular and Clinical Ophthalmology Basel (IOB), Mittlere Strasse 91, 4031 Basel, Switzerland.
E-mail: bence.gyoergy@iob.ch

hydrolysis and disassembly.[27] In some models the C-terminal region of torsinA appears to be involved in oligomerization with torsinA, LULL1, and LAP1, and interaction with nesprin-3.[3,15,28] The mutant form of torsinA appears to be unstable[29] with diminished binding to LAP1 and LULL1, and reduced activation of ATPase.[3,28] When overexpressed, mutant torsinA promotes formation of ER-derived inclusions reflecting torsinA abnormality, with deletions within the C-terminal domain preventing the development of inclusions.[30]

For those affected by DYT1 dystonia, our hypothesis has been that the incorporation of even one mutant torsinA molecule into the hexamer (depending on the model) can act in a dominant-negative manner to reduce ATPase activity.[24] By reducing the amount of mutant torsinA or its ability to participate in the hexamer, it might be possible to normalize torsinA activity at the level of haplosufficiency. Using allele-specific CRISPR-Cas9 targeting to selectively disrupt the coding sequence of the mutant allele, we sought to disrupt the C-terminal region of the mutant protein to eliminate interactions with wild-type (WT) torsinA.[31] In order to selectively target the mutation in torsinA at the genomic level, we used an engineered Cas9 from *Streptococcus pyogenes* (SpCas9-VRQR).[32] In DYT1, the in-frame GAG deletion generates a sequence (AGAT) that is recognized by the SpCas9-VRQR variant as its protospacer-adjacent motif (PAM) site. Therefore, for the DYT1 heterozygous condition, SpCas9-VRQR was a suitable alternative to increase the genome editing precision of the mutant allele. Selective disruption of the mutant allele, with loss of C-terminal amino acids, was achieved in DYT1 fibroblasts, resulting in a reduction of total levels of torsinA and a normalization of release of replicating HSV from cells.

RESULTS

Efficiency of Selective Knockout of Mutant Allele in Culture

DYT1 is caused by a heterozygous GAG deletion (c.907-909delGAG) in the last (5th) exon of the *TOR1A* gene. The GAG deletion results in the loss of one of two consecutive glutamate residues in the torsinA C-terminal (Glu303del). To selectively inactivate the mutant allele, we designed guide RNAs (gRNAs) targeted to the GAG deletion, which creates a PAM (NGAT) suitable for the SpCas9-VRQR variant[32] (Figure 1A). Fibroblasts from DYT1 patients were transfected using nucleofection with plasmids encoding SpCas9-VRQR-2A-EGFP and one of three gRNAs targeted to the mutant allele. After 3 days, genomic DNA was isolated and the *TOR1A* locus was amplified using PCR. The PCR product was purified and submitted for deep sequencing. Data analysis has been performed similarly to previous studies using the CRISPResso2 tool.[33–36] Even without selection for EGFP-positive cells, it was apparent that the H3 gRNA showed highest efficiency of *TOR1A* disruption (8.89% modified reads) (Figure 1B). Indel formation using SpCas9-VRQR and the H3 gRNA was also detectable in the Sanger sequence traces (Figure 1C). Analysis of editing using CRISPResso2 revealed that the most efficient targeting of the mutant allele was detectable with the H3 gRNA, as represented by the percentage of each base pair in a given position around the cleavage site (Figure 1D) and the quantification of individual reads containing different insertion and deletion mutations (indels) (Figure 1E). The quantification revealed that CRISPR-mediated edits occurred predominantly on the mutant allele as compared to the WT allele (in the DYT1_CRISPR-H3 gRNA condition, 46.65% of reads correspond to the WT allele and 36.89% to the mutant allele, suggesting that the remaining reads are CRISPR edits occurring mostly in the mutant allele) (Figure 1E).

We next validated CRISPR-Cas9-mediated genome editing efficiency in five DYT1 patient fibroblasts transfected with plasmids encoding SpCas9-VRQR-2A-EGFP and the H3 gRNA. To enrich the DYT1 fibroblast population with a disrupted mutant allele, cells were sorted by FACS (72 h after nucleofection) for expression of EGFP to ensure that they had been successfully transfected with the Cas9 construct. After recovery of sorted cells, genomic DNA was isolated and the region of interest was amplified by PCR. PCR products were analyzed by Sanger sequencing and next-generation sequencing (NGS) (Figure 2A). Quantification of reads aligned to the WT and mutant *TOR1A* (DYT1) alleles for each sample confirmed high editing efficiency of the mutant allele compared to the WT (Figure 2B). The CRISPResso2 analysis showed an average of 82% disruption of the mutant allele and around 21% indel of the WT allele (Figure 2C). These observations are consistent with the ability of SpCas9-VRQR to exhibit modest activity against sites with NGGN or shifted NNGAG PAMs (present in the WT allele), as shown in previous PAM profiling data for SpCas9-VQR (a parental variant of SpCas9-VRQR).[37]

The most common non-homologous end joining (NHEJ)-mediated repair was a deletion of a single G 7 bp 5′ to the mutant GAG deletion (62.48%) (Figures 2B and 2D), which would result in a frameshift leading to a premature stop codon and consequently a truncated torsinA protein lacking the last 30 aa of the C terminus (Figure 2E). Thus, rather than the normal 332-aa torsinA, the edited mutant protein would be predicted to be 302 aa long (d303–332 for $torA_{302}$) lacking functional residues/motif, including the cysteine residue (C319), the sensor 2 motif (^{318}GCK^{320}) known for its redox sensing activity, and the association with the ATP binding site structural conformation (Figure 2E), as well as potential torsinA binding sites for its partners, LULL1 and LAP1.[10]

Predicted Structural Features and Molecular Dynamics of Truncated TorsinA ($torA_{302}$)

Since the expected protein after CRISPR-Cas9 editing would be a truncated form (lacking the last 30 aa in the C-terminal) of torsinA, we performed structural prediction analysis to investigate the stability and functionality of the truncated protein and whether it would still be able to incorporate into a hexamer.[27] The structural modeling of torsinA has been previously described[2,3] and was used as a reference to analyze the consequences of the C-terminal truncated protein predicted as a result of CRISPR-Cas9 genome editing.

The physicochemical properties used for stability analysis showed no remarkable differences comparing WT and truncated $torA_{302}$ (Figure 3A). The absence of the C terminus in $torA_{302}$ would lead to lower interface area of the chains with one salt bridge missing (Figure 3A).

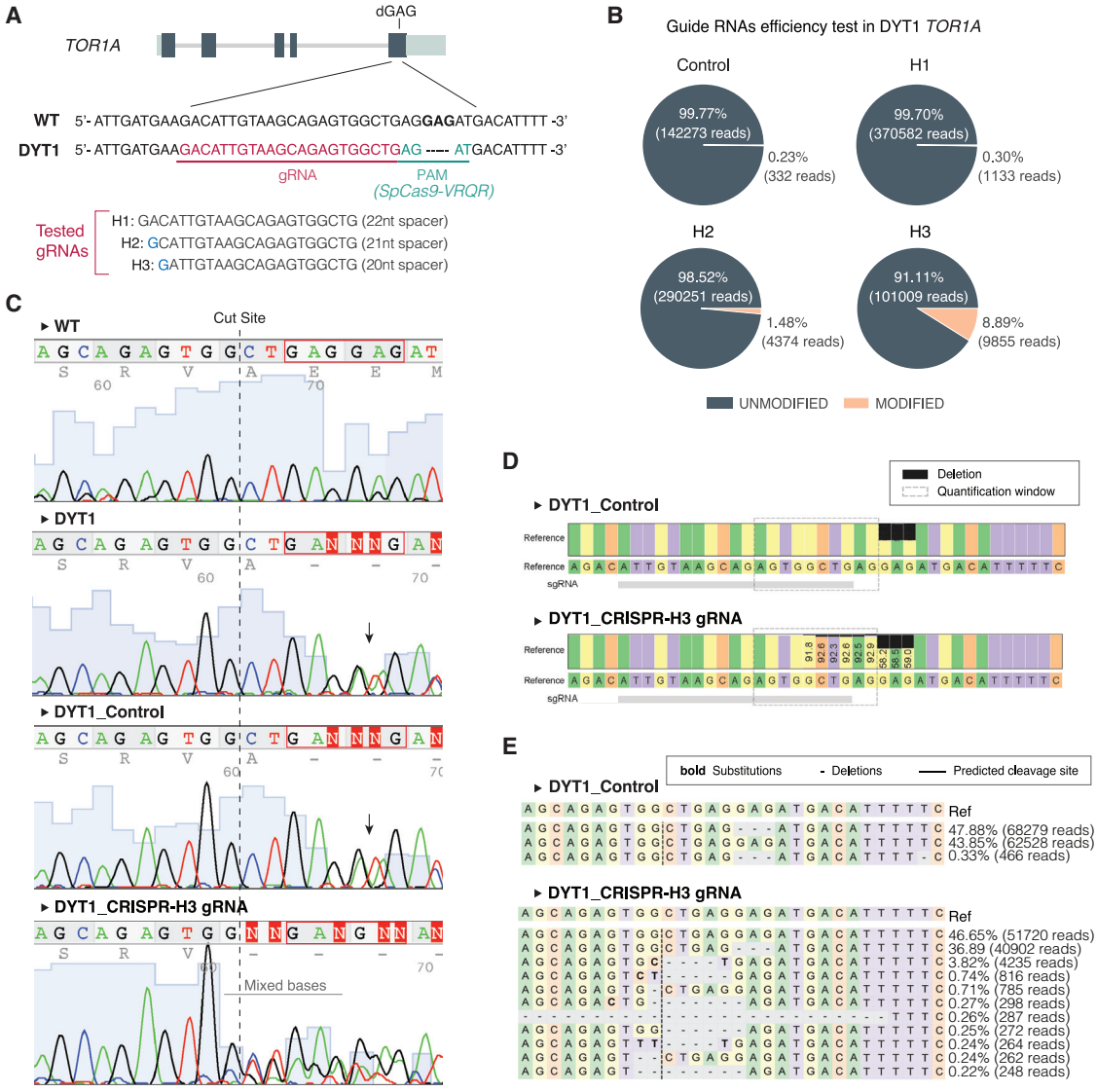

Figure 1. Targeting the Mutant *TOR1A* Gene

(A) gRNA design. The *TOR1A* gene is represented and GAG deletion (dGAG) is denoted in the 5th exon. The nucleotide sequence covering the mutation is shown for both WT and DYT1 mutant alleles with gRNA (red) and PAM site (green) for SpCas9-VRQR indicated. H1–H3 are gRNAs with different lengths. To allow expression from the U6 promoter, we added a non-annealing guanine to H2 and H3 (marked in blue). (B) gRNAs were tested in DYT1 fibroblasts and deep sequencing was performed. CRISPResso analysis was used to analyze the indel formation within a specified quantification window (5 nt on each side of cut site, area outlined with dashed line in D). The H3 gRNA showed the highest effectivity on the mutant *TOR1A*. "Control" refers to the condition in which DYT1 fibroblasts were transfected with SpCas9-VRQR only. (C) Sanger sequence traces of WT, DYT1, DYT1_Control, and DYT1_CRISPR-H3 gRNA conditions showing the base calls around the cut site (vertical black dashed line) and dGAG (GAG302–303 is highlighted in red). Blue shading behind the peaks represents base call quality. WT shows single-base peaks while DYT1 and control (no gRNA) show double peaks (arrow) due to the heterozygosis of the dGAG leading to a frameshift in one of the alleles. The DYT1_CRISPR-H3 gRNA sequence shows mixed peaks as a result of the CRISPR edits. (D and E) CRISPResso analyses showing in (D) the nucleotide percentage quantification in a given position (quantification window is highlighted with dashed gray lines), and in (E) the sequence reads aligned to the WT reference allele and percentage/total reads of indel for the DYT1_Control and DYT1_CRISPR-H3 gRNA conditions. The alignment also includes reads with indels outside of the quantification window. Reads below 0.2% frequency are not represented.

Given that the torsinA C terminus contributes to the LULL1-torsinA interface, the representation of the torA$_{302}$-LULL1 complex showed that this interface would be impaired (Figure 3B). The consequence would be consistent with the proposed analysis that the lack of the torsinA C terminus reduces cofactor (LAP and LULL1) binding and ATPase induction.[3,26,28] It would also compromise the binding of torsinA to other partners such as nesprin-3, as previously described.[15] The molecular dynamic simulation analysis revealed

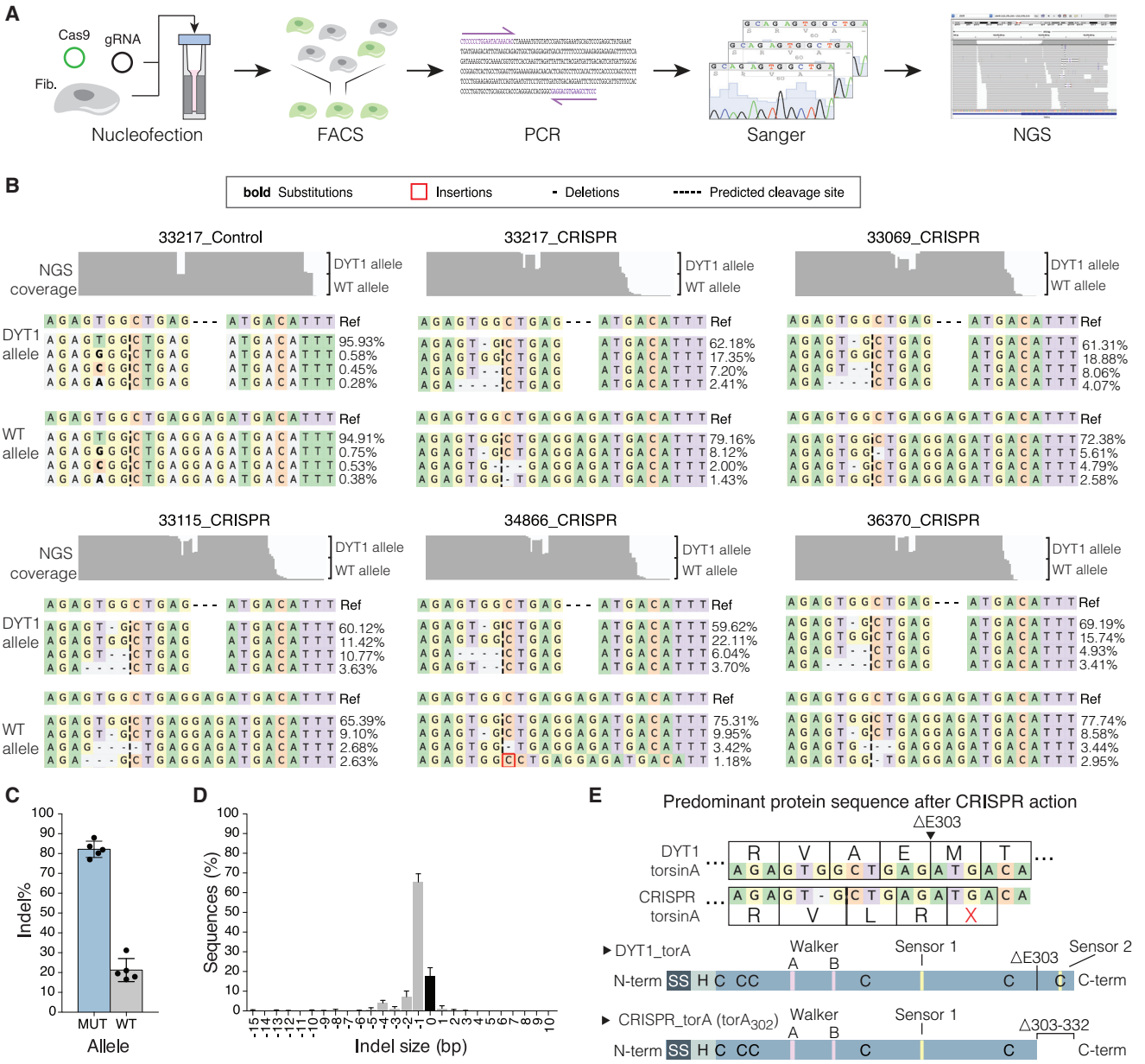

Figure 2. CRISPR-Mediated Changes in DYT1 Fibroblasts

(A) Experimental pipeline of CRISPR approach and analysis. (B) Indel quantification in WT and mutant alleles of five different fibroblasts lines (CRISPR represents DYT1 lines treated with VRQR-Cas9 and H3-gRNA) and one line treated only with VRQR-Cas9 (33217_Control). Top gray images represent NGS coverage (visualized using IGV) and show a white gap in half of the reads comprising the DYT1 allele. Bottom charts represent percentage of reads of individual indel in the DYT1 and WT alleles (CRISPResso analysis). (C) Using the VRQR-Cas9 and H3 gRNA there was a high efficiency of targeting the mutant as compared to the WT allele. (D) The most common indel (62.5%, 3.9%) using the H3 gRNA was a single base pair deletion resulting in a frameshift before the dGAG. (E) DYT1 and CRISPR-edited torsinA (DYT1_torA and CRISPR_torA) codon and respective amino acid sequences showing the early stop codon insertion (X) as a consequence of the most common indel (single base pair deletion). Schematic view of torsinA (DYT1_torA and CRISPR_torA) protein highlighting the signal sequence (SS) and the hydrophobic (H) domains in the N-terminal, the cysteines (C) along the AAA+ domain (light blue), and the functional motifs (Walker A and B and the sensors 1 and 2 mainly involved with ATP binding and hydrolysis). The early stop codon (CRISPR_torA) leads to a truncated form of torsinA lacking the last 30 aa in the C-terminal (d303–332, $torA_{302}$) including one cysteine residue and the sensor 2 motif. Data are expressed as mean ± SEM.

A

WT torsinA

Chains	No. of interface residues	Interface area (Å^2)	No. of salt bridges	No. of hydrogen bonds	No. of non-bonded contacts
A-B	10:13	733:700	-	3	45
B-C	11:13	717:681	1	3	42
C-D	10:13	729:699	-	2	43
D-E	11:13	770:725	-	4	49
E-F	9:12	695:665	-	3	43
A-F	14:12	680:702	-	3	48

torsinA$_{302}$

Chains	No. of interface residues	Interface area (Å^2)	No. of salt bridges	No. of hydrogen bonds	No. of non-bonded contacts
A-B	9:12	632:599	-	3	44
B-C	10:12	610:571	-	3	40
C-D	9:12	630:591	-	2	41
D-E	10:12	656:606	-	4	48
E-F	8:11	613:576	-	3	42
A-F	12:10	578:599	-	3	46

B

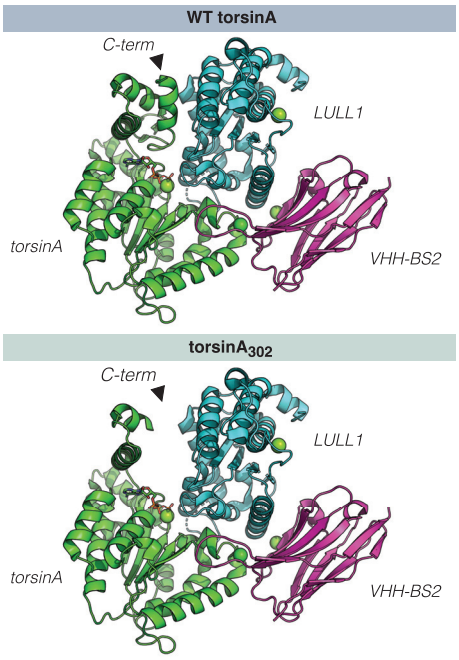

C

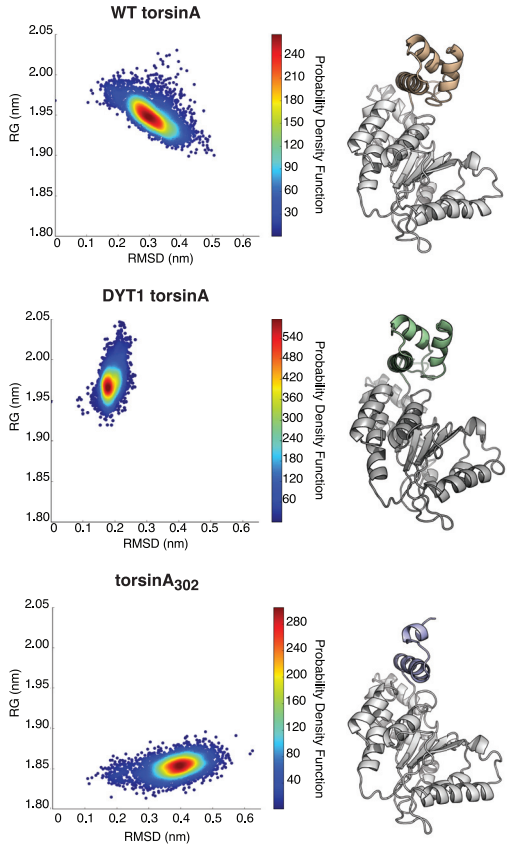

D

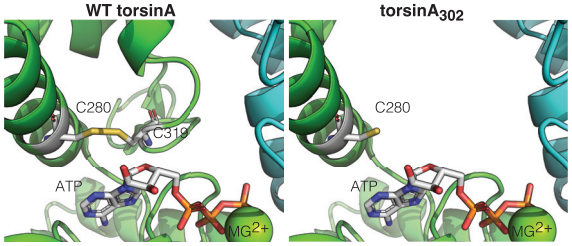

E

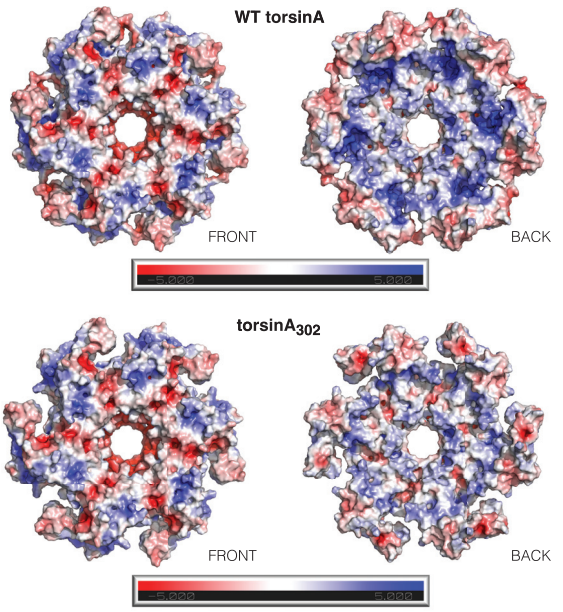

(legend on next page)

that the overall structural conformations of the mutated (dE303, DYT1 torsinA) and the truncated $torA_{302}$ are conserved when compared to the WT torsinA, except for the missing C-terminal region, which could confer a slightly lower compaction level (radius of gyration-RG) observed in $torA_{302}$ (Figure 3C). The absence of the last 30 aa in the C terminus of $torA_{302}$ is predicted to lead to a higher flexibility in the torsinA C terminus due to the loss of the disulfide bond between the residues C280 and C319 (Figure 3D). This flexibility would also compromise the ATPase site formation in torsinA hexamer predictions, as represented by the dark blue regions in the back of the WT homohexamer structure (Figure 3E). The prediction analysis showed that the homohexamer formation consisting of only truncated torsinA is still possible, but would rely more on the torsinA N-terminal region. However, this homohexamer might not be stable or functional due to the C terminus flexibility and the impairment in the ATP binding site (Figure 3E).

CRISPR-Disrupted Mutant Allele Does Not Affect *TOR1A* mRNA Levels, but Decreases TorsinA Protein Levels

As this CRISPR procedure predominantly targeted the mutant allele leading to a predicted truncated form of torsinA, we then assessed whether CRISPR treatment affected torsinA mRNA and protein levels, while also monitoring for any additional effects on torsinB (*TOR1B*). qPCR data showed no difference in *TOR1A* and *TOR1B* mRNA expression levels between WT, DYT1, control (no gRNA), and CRISPR conditions (Figure 4A). By using an antibody targeting the N-terminal region of torsinA (DM2A8), we confirmed that DYT1 patient fibroblasts have a lower amount of torsinA compared to WT fibroblasts, as noted by others,[14] and that while the control condition has the same level of torsinA as in DYT1 cells, there is a significant decrease in total torsinA in the edited cells significantly below that in the DYT1 cells (Figures 4B–4D). Incubation of protein lysates with PNGase F, an N-glycosidase, reduced torsinA molecular weight to an apparent mass of 33 kDa in all four groups (Figure 4B; Figure S1), confirming the glycosylation status of torsinA.[38,39] This CRISPR-Cas9-mediated decrease in torsinA levels suggests that the truncated mutant torsinA is unstable and degraded.

Does Disruption of the Mutant *TOR1A* Allele Normalize Function in DYT1 Patient Fibroblasts?

Assuming that the mutant *TOR1A* allele acts as a dominant-negative to suppress torsinA activity, we considered the possibility that disruption of the mutant allele could "normalize" cellular functions that depend on torsinA. Based on findings by ourselves and others, torsinA is involved in replication of HSV-1, at least in part, during the egress of newly generated capsids through the NE into the cytoplasm.[20,22,40] This would predict relatively lower HSV genome copies inside WT cells and higher numbers in the WT cell supernatant as compared to DYT1 cells, as was observed (Figures 5A–5C). CRISPR-Cas9 editing of DYT1 cells decreased the relative amount of HSV DNA in the cells and increased the relative amount in the supernatant, making it more similar to control cells (Figures 5C and 5D; Figure S2). The difference is most evident when DYT1-edited cells are compared to their respective controls (no gRNA), since both conditions represent cells that were submitted simultaneously to all steps of the targeting process (Figure 5D). This supports normalization of torsinA function in the DYT1 cells by selective disruption of the mutant *TOR1A* allele.

DISCUSSION

There has been some debate as to whether DYT1 dystonia, caused by a GAG deletion in the coding region of one allele of *TOR1A*,[1] is due to haploinsufficiency of the functional torsinA protein or a dominant-negative effect of the mutant protein on the WT protein.[24] This study supports a dominant-negative effect with truncation of the mutant allele apparently leading to its degradation and restoration of one of the functions of torsinA in facilitating replication of HSV. Previous studies by ourselves and others[20,22,40] have shown that torsinA facilitates transit of replicating HSV capsids in the cell nucleus across the NE from whence they enter into the cytosol and exit the cell, and that mutant torsinA at endogenous levels interferes with this process in DYT1 fibroblasts. Thus, this study indicates that selective NHEJ disruption of the mutant allele at the site of the mutation can lead to an increase in normal torsinA activity in cultured DYT1 fibroblasts. Supporting our findings, other studies have shown that it is possible to selectively silence the mutant mRNA using small interfering RNA (siRNA), providing evidence that this approach normalizes the DYT1 phenotype and that mutant torsinA acts in a dominant manner by inhibition of WT torsinA activity.[41,42]

It is remarkable that so few mutations have been found in the *TOR1A* locus encoding torsinA. If haploinsufficiency of this protein could cause a medical problem, more mutations, especially nonsense mutations throughout the protein, would be expected. Instead, our data support a dominant-negative mechanism whereby mutations/variants in the coding region of this gene present together with a WT allele act

Figure 3. Predicted Structural Changes in TorsinA Due to DYT1 Mutation and Its Elimination by CRISPR

(A) Physicochemical properties of WT and predicted torsinA protein after CRISPR ($torsinA_{302}$, $torA_{302}$) structures. (B) Representation of (WT and $torA_{302}$) torsinA (green)-LULL1 (blue) complex stabilized by VHH-BS2 (purple) based on Demircioglu et al.[3] Missing C-terminal in $torA_{302}$ is predicted to compromise binding to LULL1. (C) Molecular dynamic simulation analysis of different predicted torsinA structures represented on the right side (WT torsinA, DYT1 mutant torsinA, and $torA_{302}$). The majority of the protein structure (in gray) is conserved in all three torsinA versions with main differences in the C-terminal region of $torA_{302}$ (purple) when compared to DYT1 torsinA (green) and WT torsinA (brown). RMSD, root-mean-square deviation; RG, radius of gyration. (D) Cysteines C280–C319 interaction featured in the ATP binding site (C-terminal) of torsinA. C319 is missing in $torA_{302}$, which can impact the conformation of the ATP binding site. (E) The most stable torsinA conformation calculated in the molecular dynamic simulation for WT and $torA_{302}$ was used to prepare the homohexamer simulations. Color scale represents charge level (red is more negatively charged and blue is more positively charged regions). Predicted structures of homohexamers of WT torsinA and $torA_{302}$ (front and back views). In the back view, the dark blue areas correspond to the ATP binding sites, which are not present in the $torA_{302}$ homohexamer.

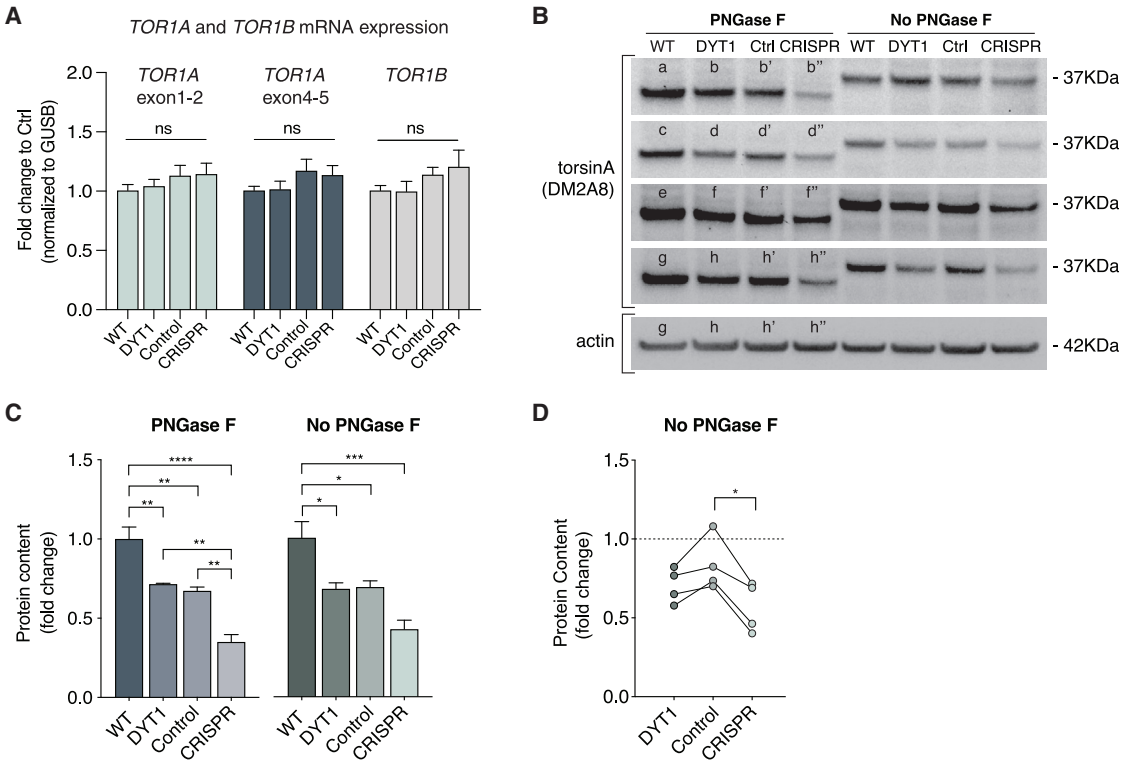

Figure 4. CRISPR-Mediated Mutant Allele Disruption Does Not Affect *TOR1A* mRNA Levels, but Decreases TorsinA Protein Levels

(A) *TOR1A* (exon junctions 1–2 and 4–5) and *TOR1B* mRNA expression in WT (n = 5), DYT1 (n = 4), control (n = 4), and CRISPR (n = 4) fibroblasts. Data are expressed as mean ± SEM. (B) Representative immunoblot images of torsinA protein levels (DM2A8 antibody) in fibroblast lysates incubated or not with PNGase F. Each letter represents a different sample; the single quotation (') and double quotation (") represent, respectively, the control and CRISPR conditions for the corresponding DYT1. The samples sequence of the "No PNGase F" condition is the same as indicated in the "PNGase F" in each gel. Actin was used as loading control for each individual gel. (C) Densitometry analysis of immunoblot shown in B. Data are expressed as mean ± SEM. (D) Immunoblot density analysis using average of three independent experiments without PNGase F treatment. Fold change was calculated relative to the WT (dashed line). (C and D) One-way (C) or repeated measures (D) ANOVA was performed to compare groups. Tukey's multiple comparison tests were performed when ANOVA showed a significant effect. *p < 0.05, **p < 0.01, ***p < 0.001, ****p < 0.0001.

in concert to decrease functional torsinA in this heterozygous state to below 50% levels. The limited number of mutations/variants found in *TOR1A* suggests that most have no pathophysiologic effects in the heterozygous state, and loss of function in the homozygous state, at least in the mouse, is usually associated with embryonic lethality.[14,43] In contrast, several recently described mutations in *TOR1A*, either homozygous (p.R288*, G318S, p.E303del) or compound heterozygous mutations (p.E303del/p.T321Rfs*6), have been described in infants or young children with severe congenital joint fracture (arthrogryposis) and developmental delay.[44–46] From these data, it appears that haploinsufficiency is not pathologic, whereas >50% loss of torsinA activity can cause dystonia or be incompatible with normal development, depending on the extent of loss. Moreover, most of the few heterozygous mutations/variants associated with a movement disorder phenotype occur in the C-terminal region of the gene.[2] Interestingly, CRISPR disruption of the mutant *TOR1A* allele in this study most commonly results in a truncated protein lacking 30 aa from the C-terminal region. Very few other truncating mutations have been described in gnomAD (overall allele frequency of 1.1×10^{-4}); all are heterozygous, and it is not clear if any are pathogenic.[47]

Our hypothesis has been that only mutations in torsinA that are compatible with its incorporation into the hexamer with normal torsinA, and thus interfere with ATPase activity, cause pathophysiologic consequences in a dominant fashion. Extensive structural predictions of the truncated version of torsinA by CRISPR-Cas9 editing, as well as WT and mutant torsinA, indicate that the resulting loss of a disulfide bond in the C-terminal region would lead to more flexibility, thus compromising interactions with other monomers in the hexameric structure and destabilizing binding of ATP. The reduced interaction with other monomers may account for the apparent increased susceptibility of the truncated version to degradation. In turn, this would lead to more hexamers composed entirely of WT torsinA in the DYT1 CRISPR-Cas9-edited cells, as compared to a mixture of mutant and WT torsinA in non-edited cells.

CRISPR editing of the genome is rapidly becoming a new modality in research and clinical medicine.[48] With respect to neurologic diseases, it is still early to claim to what extent gene repair can be carried out in non-replicating neurons *in vivo* to lead to effective symptom amelioration. At present, a study in a mouse model of inherited hearing loss

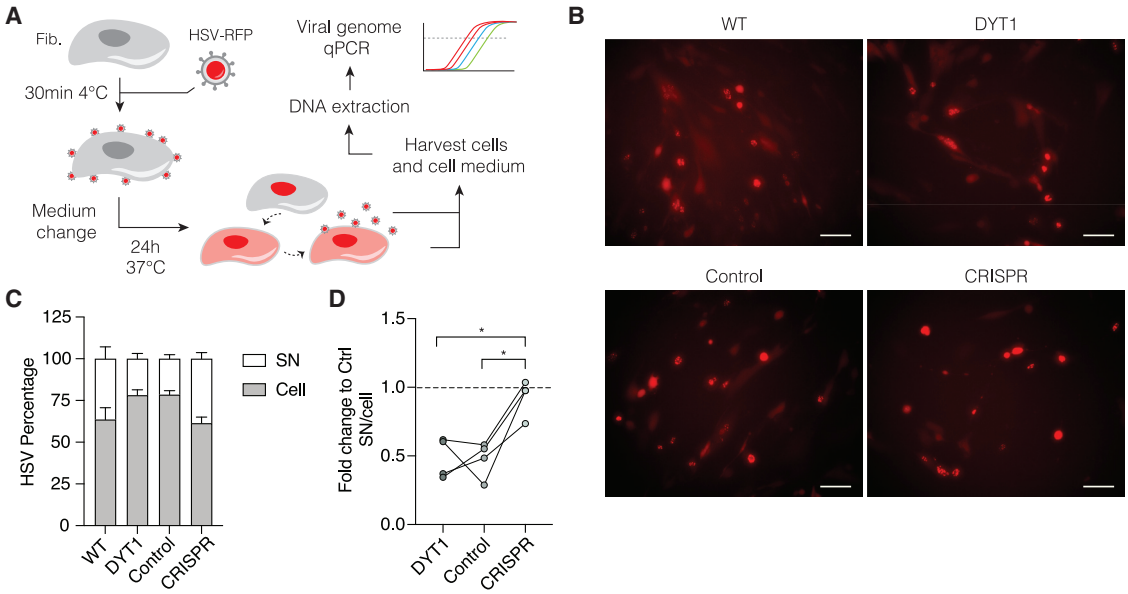

Figure 5. Normalization of HSV Replication in DYT1 Cells after CRISPR Disruption of the Mutant Allele

(A) Experiment schematic. Fibroblasts of different genotypes were infected with HSV-mRFP at an MOI of 10 and infection synchronized at 4°C for 30 min. Medium was changed, and plates were incubated at 37°C. HSV genome copies were assessed in DNA extracted from cells and in cell-free conditioned medium (supernatant [SN]) after 24 h of infection. (B) Representative micrographs of HSV-mRFP infected fibroblasts of each group (24 h post-infection). Scale bars, 100 μm. (C) HSV genome copies percentage in cell and SN of three independent experiments (WT, n = 5; DYT1, n = 4; control, n = 4; CRISPR, n = 4). Data are expressed as mean ± SEM. (D) Fold change of the SN/cell ratio was calculated relative to the control (dashed line). Repeated measures ANOVA ($p = 0.01$) was performed to compare DYT1, control, and CRISPR groups. Tukey's multiple comparison tests were further performed. *$p < 0.05$.

provides strong evidence that disrupting a dominantly acting mutation through NHEJ using a single gRNA and Cas9, leaving the WT allele intact, can restore physiologic function.[34] New studies on adapting the CRISPR system for gene editing have provided promising advances for genetic diseases, including its use in non-dividing cells such as post-mitotic mouse cortical neurons and sensory and hair cells in the mouse inner ear.[49–51] These studies have used catalytically modified components of CRISPR to enable the conversion of one base into another without inducing double-stranded break (DSB) known to create undesired byproducts. More recently, this genome editing became more precise with a method that can both recognize the target site and insert the desired nucleotide without DBS or donor DNA.[51] Improvements in this technique have become the next focus: to increase the base editing purity, to reduce the detectable rate of indel formation and off-targeting, to increase *in vivo* delivery to target-specific tissues, and to increase precise base editing of genetic diseases. Although the gRNAs and mutant Cas9 described herein are mostly selective for disrupting the mutant *TOR1A* allele in a predictable mode, leaving the WT allele largely intact, it remains to be determined how effective this could be in targeting human neurons and whether off-target effects would compromise therapeutic intervention.

DYT1 is thought to be caused by dysfunction of corticostriatal synapses, which compromises their plasticity,[52] due at least in part to hypercholinergic tone,[53] although how that is caused by deficit in torsinA function is not known.[54] Corroborating the positive effects of mutant-specific silencing by siRNA,[41,42] the present studies suggest the possibility of stereotactic injection of adeno-associated virus (AAV) vectors or other vehicles carrying the gRNA and Cas9 designed to be selective for the mutant *TOR1A* allele, to disrupt it in hopes of normalizing function of these neurons, which could be evaluated electrophysiologically in a DYT1 mouse model (e.g., see Goodchild et al.[14]). With AAV vectors advancing to products for neurologic and eye diseases,[55] this strategy presents a potentially "single shot," new mode of therapeutic intervention in DYT1dystonia.

MATERIALS AND METHODS

Cell Culture

Coded primary human skin fibroblasts from DYT1 patients (33069, 33115, 33217, 34866, 36370) and healthy controls (33114, 33430, 33362, 35628, 33113, referred to here as "WT" in distinction from the "control" condition of the CRISPR approach) were obtained and used through a protocol approved by the Partners Human Research Committee (2009p-001500). Informed consent was obtained from all subjects. All fibroblasts were cultured in Dulbecco's modified Eagle's medium (DMEM) with high glucose supplemented with 20% fetal bovine serum (FBS) (Thermo Fisher Scientific, Waltham, MA, USA) and 1% penicillin/streptomycin (Invitrogen, Carlsbad, CA, USA) (DMEM/20). Cultures were negative for mycoplasma contamination, as assessed using a PCR mycoplasma detection kit (Applied Biological Materials, Richmond, BC, Canada).

gRNA Design and Plasmid

The DYT1 GAG deletion in exon 5 of the *TOR1A* human gene (c.907_909delGAG; p.Glu303del; ΔE 303) creates a PAM site (NGAT) suitable for the *Streptococcus pyogenes* Cas9-VRQR (SpCas9-VRQR) variant.[32] Three gRNAs (H1–H3) were designed adjacent to the PAM site and tested for efficiency. Plasmid encoding the gRNA under a U6 promoter (cloned into MLM3636) and the plasmid expressing Cas9-VRQR-EGFP under a CAG promoter (MSP2532, pCAG-hSpCas9-VRQR-NLS-FLAG-P2A-EGFP)[32] were used in this study.

Nucleofection of Plasmids

One milliliter of DMEM with 20% FBS (DMEM/20) per well in a six-well plate was prewarmed. One million fibroblasts were resuspended in 100 μL of primary cell nucleofection solution (80 μL of P2 solution + 20 μL of supplement of a P2 Primary Cell 4D-Nucleofector X kit). Cells were mixed with 1 μg of SpCas9-VRQR-2A-EGFP plasmid and 1 μg of gRNA and transferred to a nucleofection cuvette. Cells were electroporated using a 4D-Nucleofector core unit (Lonza, CZ167 program). After nucleofection, prewarmed DMEM/20 was used to transfer transfected cells into a six-well plate. Transfection with only SpCas9-VRQR (no gRNA) was used as a control condition (termed Control). After 72 h, EGFP-positive fibroblasts underwent fluorescence-activated cell sorting (FACS; FACSAria) and were cultured until confluent. Genome editing with CRISPR was performed in five DYT1 lines, but because line 36370 did not completely recover after FACS that DYT1 line was not used in experimental analysis.

Analysis of Gene Editing Outcomes

Genomic DNA of sorted CRISPR-transfected fibroblasts were isolated using a DNAeasy Tissue and Blood kit (QIAGEN, Hilden, Germany), and PCR of the DYT1 mutation region was performed using Phusion high-fidelity DNA polymerase (New England Biolabs, Ipswich, MA, USA), with the following primers: forward, 5′-CTCCCCCTGGAA TACAAACA-3′, reverse, 5′-GGAGCTGGCTCCTTCCTTCT-3′. PCR products were purified with the PCR product purification kit (QIAGEN) and submitted for Sanger sequencing with the same primers. Purified PCR products were submitted to targeted deep sequencing (MGH DNA Core, Boston, MA, USA), and quantification of indels was performed using CRISPResso2.[36] In parallel, the Galaxy web platform was used for alignment of NGS data to the reference genome, and the Integrative Genomics Viewer (IGV) was used for NGS data visualization.[56,57]

Predicted Structural Features of CRISPR-Edited TorsinA ($torA_{302}$)

Sequencing analysis of genome editing events resulting from treatment with SpCas9-VRQR revealed a 1-bp deletion as the most common indel in fibroblasts. The 1-bp frameshift is predicted to lead to a stop codon positioned at aa 302 with predicted formation of torsinA missing the last 30 aa in the C-terminal region (termed $torA_{302}$). Structural analyses were performed to compare WT, DYT1, and $torA_{302}$ hexamers. The crystal structures of torsinA WT and DYT1 were obtained from the Protein Data Bank (PDB), using PDB: 5J1S and 5J1T, respectively.[3] The $torA_{302}$ structure was built based on the WT structure. All Poisson-Boltzmann calculations were done using the Adaptive Poisson-Boltzmann Solver (APBS)[58] PyMOL plugin.

Molecular Dynamics Simulations

Molecular dynamics simulations were performed for three torsinA systems: (1) WT, (2) DYT1, and (3) $torA_{302}$. Amber99SB force field[59] implemented in GROMACS 2016.3[60] was used to describe the atoms of the system. Periodic bound conditions were applied, and the numbers of particles, pressure, and temperature were maintained constant (NPT ensemble) during the whole production phase. The V-rescale[61] thermostat was used to maintain the system at constant temperature using a coupling time of 0.1 ps, and the Berendsen barostat[62] was applied to ensure that the system pressure was maintained at 1 bar. The LINCS algorithm[63] was implemented in order to constrain all of the covalent bonds involving hydrogen atoms and the system evolved in time in steps of 2 fs. van der Waals interactions were computed using a 12 Å cutoff. The particle mesh Ewald method was applied to calculate electrostatic contributions in a grid with 1.2 Å spacing. The macromolecule was fully solvated using the TIP3P model[64] in a cubic box extending 10 Å from the macromolecule surfaces. The systems were submitted to steepest-descent energy minimization up to a tolerance of 1,000 kJ/mol/nm in order to remove close contacts of van der Waals forces. The equilibration phase was performed in two steps: (1) an NVT equilibration for 500 ps, followed by (2) an NPT equilibration step lasting 1,000 ps before the production phase, lasting for 100 ns.

Preparation of Cell Lysate and Western Blots

For total cell lysates, cells were suspended in radioimmunoprecipitation assay (RIPA) buffer (150 mM NaCl, 50 mM Tris [pH 7.5], 1% Nonidet P-40 [NP40], 0.5% deoxycholate, 0.1% SDS) with protease inhibitor (cOmplete, Mini, EDTA-free tablets, Roche, Indianapolis IN, USA). Twenty micrograms of total protein from each lysate was prepared in NuPage lithium dodecyl sulfate (LDS) sample buffer (Thermo Fisher Scientific) and heated at 95°C for 10 min before undergoing electrophoresis. Deglycosylation of total cell lysate was performed by using PNGase F (New England Biolabs, Ipswich, MA, USA), according to the manufacturer's instructions. In brief, 20 μg of total cell lysate was combined in glycoprotein denaturing buffer and denatured by heating at 100°C for 10 min. GlycoBuffer 2, NP40, and PNGase F were added and samples were incubated at 37°C for 1 h. Non-treated samples were included following the same steps, except that PNGase was not added to the reaction. LDS sample buffer was added to processed lysates and heated at 95°C for 10 min before resolution by electrophoresis.

Cell lysates were resolved by electrophoresis on Novex Bolt Bis-acrylamide (4%–12%) gels and transferred to nitrocellulose membranes. Membranes were blocked with 5% milk in Tris-buffered saline with Tween 20 (TBST; 150 mM NaCl, 50 mM Tris [pH 7.9], 0.5% Tween 20) and incubated overnight in primary antibodies diluted in 5% milk

in TBST. Membranes were washed three times in TBST and incubated with horseradish peroxidase (HRP)-conjugated secondary antibodies, with labeled proteins visualized via chemiluminescence using SuperSignal West Pico substrate (Thermo Fisher Scientific). Antibodies used for western blotting were as follows: mouse anti-torsinA (DM2A8 raised against MBP-torA51-324,[4] and confirmed to recognize specifically the torsinA N-terminal; data not shown), mouse anti-β actin (A5544, Sigma-Aldrich, St. Louis, MO, USA, 1:2,000), and HRP-conjugated anti-mouse immunoglobulin G (IgG; NA 931, Amersham Pharmacia Biotech, 1:1,000).

HSV Infection and Quantitation

Virus stock of HSV-VP26mRFP was prepared as described, and titer was calculated as plaque-forming units (PFU/μL).[65] Fibroblasts seeded in 12-well plates (10^5 cells/well) were infected with virus at the multiplicity of infection (MOI) of 10. Cells were incubated at 4°C for 30 min and media were changed to DMEM/20 for 24 h. Conditioned media were collected, centrifuged at 300 × *g* for 4 min, and supernatant was collected. Cells were trypsinized, centrifuged at 300 × *g* for 4 min, and the pellet was saved. DNA was extracted from supernatant and cell pellet using a DNeasy Tissue and Blood kit (QIAGEN, Hilden, Germany), according to the manufacturer's instructions. DNA concentration was measured with Qubit (Thermo Fisher Scientific) using a high sensitivity (HS) DNA kit (Qubit 1× double-stranded DNA [dsDNA] HS assay kit). HSV genome copies were determined using 0.2 ng of DNA per reaction and based on the internal standard curve prepared with HSV virus stock serially diluted in the range of 100–100,000 genome copies. The PCR mix was prepared with SYBR Green master mix (Thermo Fisher Scientific) with primers for the tegument k (tk) gene (forward, 5′-AGGCATGCCCATTG TTATCTG-3′, reverse, 5′-GAGACAATCGCGAACATCTAC-3′). qPCR was run on the QuantStudio 3 real-time PCR system (Thermo Fisher Scientific) using 40 cycles.

qPCR

Reverse transcription of isolated RNA was performed using a SuperScript VILO cDNA kit (Thermo Fisher Scientific). Quantitative real-time PCR was performed using Power SYBR Green master mix (Thermo Fisher Scientific) or TaqMan master mix (Thermo Fisher Scientific). Expressions of torsin family 1 member A (*TOR1A*) and torsin family 1 member B (*TOR1B*) were detected using TaqMan primers (*TOR1A* exon-exon junction 1–2, Hs01115608_m1; *TOR1A* exon-exon junction 4–5, Hs0164427_m1; *TOR1B* exon-exon junction 2–3, Hs00248082_m1) and TaqMan gene expression master mix (Thermo Fisher Scientific) on the QuantStudio 3 real-time PCR system (Thermo Fisher Scientific). Glucuronidase, beta (*GUSB*; Hs009396_m1) was used as housekeeping gene for data normalization.

Statistical Analysis

Data are expressed as mean ± SEM or individual values. Statistical analyses were performed using GraphPad Prism 8 software. One-way or repeated-measurement analysis of variance (ANOVA), followed by Tukey's multiple comparison test, was applied to compare experimental groups. Statistical significance was defined as $p < 0.05$.

SUPPLEMENTAL INFORMATION

Supplemental Information can be found online at https://doi.org/10.1016/j.omtn.2020.05.009.

AUTHOR CONTRIBUTIONS

B.G., L.C., B.P.K., D.C.B., and X.O.B. designed research. L.C., B.G., P.S.C., J.K.J., W.A.E., L.F.S.M.T., and O.N.d.S. performed experiments. L.C., B.G., P.S.C., S.P.G., L.F.S.M.T., and O.N.d.S. analyzed data. L.C., B.G., P.S.C., L.J.O., D.C.B., and X.O.B. wrote the paper.

CONFLICTS OF INTEREST

B.P.K. and J.K.J. are inventors on various patents and patent applications that describe gene editing and epigenetic editing technologies. B.P.K. consults for Avectas, Inc. and is an Advisor for Acrigen Biosciences. J.K.J. has financial interests in Beam Therapeutics, Editas Medicine, Excelsior Genomics, Pairwise Plants, Poseida Therapeutics, Transposagen Biopharmaceuticals, and Verve Therapeutics (formerly known as Endcadia). J.K.J.'s interests were reviewed and are managed by Massachusetts General Hospital and Partners HealthCare in accordance with their conflicts of interest policies. J.K.J. is a member of the Board of Directors of the American Society of Gene and Cell Therapy.

ACKNOWLEDGMENTS

We thank Xuan Zhang and Massimo Aufiero for the technical support, and Trisha Multhaupt-Buell for diligent management of the MGH DYT1 fibroblast bank. We thank Roberta Beauchamp, Vijaya Ramesh, and Jeffrey Hewett for providing unpublished data on antibody DM2A8. This work was supported by NIH/NINDS grants P30 NS045776 (to X.O.B.) and P01 NS087997 (to X.O.B. and L.J.O.), a prize from the Bachmann-Strauss Dystonia and Parkinson Foundation and the Michael J. Fox Foundation (to X.O.B.), and Tyler's Hope for a Dystonia Cure (to X.O.B. and D.C.B.). B.G. was an Edward R. and Anne G. Lefler Center postdoctoral fellow. L.C. is a Dystonia Medical Research Foundation postdoctoral fellow. O.N.d.S and L.F.S.M.T acknowledge support from Coordenação de Aperfeiçoamento de Pessoal de Nível Superior-Brasil (CAPES), Finance Code 001. O.N.d.S is supported by grants TO2054-2551/13-0 from FAPERGS and 304704/2018-0 from CNPq. L.F.S.M.T is supported by grants 407537/2018-0 from CNPq and 10901360 from the University of Taquari Valley (Univates). B.P.K. is supported by NIH grants R00-CA218870 and P01-HL142494, a Career Development Award from the American Society of Gene & Cell Therapy, and the Margaret Q. Landenberger Research Foundation. J.K.J. is supported by grants from the NIH (R35 GM118158, R01 CA211707, and R01 CA204954) and the Desmond and Ann Heathwood MGH Research Scholar Award.

REFERENCES

1. Ozelius, L.J., Hewett, J.W., Page, C.E., Bressman, S.B., Kramer, P.L., Shalish, C., de Leon, D., Brin, M.F., Raymond, D., Corey, D.P., et al. (1997). The early-onset torsion dystonia gene (*DYT1*) encodes an ATP-binding protein. Nat. Genet. *17*, 40–48.

2. Hettich, J., Ryan, S.D., de Souza, O.N., Saraiva Macedo Timmers, L.F., Tsai, S., Atai, N.A., da Hora, C.C., Zhang, X., Kothary, R., Snapp, E., et al. (2014). Biochemical and

cellular analysis of human variants of the DYT1 dystonia protein, torsinA/TOR1A. Hum. Mutat. *35*, 1101–1113.

3. Demircioglu, F.E., Sosa, B.A., Ingram, J., Ploegh, H.L., and Schwartz, T.U. (2016). Structures of TorsinA and its disease-mutant complexed with an activator reveal the molecular basis for primary dystonia. eLife *5*, e17983.
4. Hewett, J., Ziefer, P., Bergeron, D., Naismith, T., Boston, H., Slater, D., Wilbur, J., Schuback, D., Kamm, C., Smith, N., et al. (2003). TorsinA in PC12 cells: localization in the endoplasmic reticulum and response to stress. J. Neurosci. Res. *72*, 158–168.
5. Naismith, T.V., Heuser, J.E., Breakefield, X.O., and Hanson, P.I. (2004). TorsinA in the nuclear envelope. Proc. Natl. Acad. Sci. USA *101*, 7612–7617.
6. Goodchild, R.E., Buchwalter, A.L., Naismith, T.V., Holbrook, K., Billion, K., Dauer, W.T., Liang, C.C., Dear, M.L., and Hanson, P.I. (2015). Access of torsinA to the inner nuclear membrane is activity dependent and regulated in the endoplasmic reticulum. J. Cell Sci. *128*, 2854–2865.
7. Hewett, J.W., Tannous, B., Niland, B.P., Nery, F.C., Zeng, J., Li, Y., and Breakefield, X.O. (2007). Mutant torsinA interferes with protein processing through the secretory pathway in DYT1 dystonia cells. Proc. Natl. Acad. Sci. USA *104*, 7271–7276.
8. Nery, F.C., Armata, I.A., Farley, J.E., Cho, J.A., Yaqub, U., Chen, P., da Hora, C.C., Wang, Q., Tagaya, M., Klein, C., et al. (2011). TorsinA participates in endoplasmic reticulum-associated degradation. Nat. Commun. *2*, 393.
9. Beauvais, G., Rodriguez-Losada, N., Ying, L., Zakirova, Z., Watson, J.L., Readhead, B., Gadue, P., French, D.L., Ehrlich, M.E., and Gonzalez-Alegre, P. (2018). Exploring the interaction between eIF2α dysregulation, acute endoplasmic reticulum stress and DYT1 dystonia in the mammalian brain. Neuroscience *371*, 455–468.
10. Zhu, L., Millen, L., Mendoza, J.L., and Thomas, P.J. (2010). A unique redox-sensing sensor II motif in torsinA plays a critical role in nucleotide and partner binding. J. Biol. Chem. *285*, 37271–37280.
11. Rose, A.E., Zhao, C., Turner, E.M., Steyer, A.M., and Schlieker, C. (2014). Arresting a torsin ATPase reshapes the endoplasmic reticulum. J. Biol. Chem. *289*, 552–564.
12. Grillet, M., Dominguez Gonzalez, B., Sicart, A., Pöttler, M., Cascalho, A., Billion, K., Hernandez Diaz, S., Swerts, J., Naismith, T.V., Gounko, N.V., et al. (2016). Torsins are essential regulators of cellular lipid metabolism. Dev. Cell *38*, 235–247.
13. Shin, J.Y., Hernandez-Ono, A., Fedotova, T., Östlund, C., Lee, M.J., Gibeley, S.B., Liang, C.C., Dauer, W.T., Ginsberg, H.N., and Worman, H.J. (2019). Nuclear envelope-localized torsinA-LAP1 complex regulates hepatic VLDL secretion and steatosis. J. Clin. Invest. *130*, 4885–4900.
14. Goodchild, R.E., Kim, C.E., and Dauer, W.T. (2005). Loss of the dystonia-associated protein torsinA selectively disrupts the neuronal nuclear envelope. Neuron *48*, 923–932.
15. Nery, F.C., Zeng, J., Niland, B.P., Hewett, J., Farley, J., Irimia, D., Li, Y., Wiche, G., Sonnenberg, A., and Breakefield, X.O. (2008). TorsinA binds the KASH domain of nesprins and participates in linkage between nuclear envelope and cytoskeleton. J. Cell Sci. *121*, 3476–3486.
16. Saunders, C.A., Harris, N.J., Willey, P.T., Woolums, B.M., Wang, Y., McQuown, A.J., Schoenhofen, A., Worman, H.J., Dauer, W.T., Gundersen, G.G., and Luxton, G.W. (2017). TorsinA controls TAN line assembly and the retrograde flow of dorsal perinuclear actin cables during rearward nuclear movement. J. Cell Biol. *216*, 657–674.
17. Pappas, S.S., Liang, C.C., Kim, S., Rivera, C.O., and Dauer, W.T. (2018). TorsinA dysfunction causes persistent neuronal nuclear pore defects. Hum. Mol. Genet. *27*, 407–420.
18. Laudermilch, E., and Schlieker, C. (2016). Torsin ATPases: structural insights and functional perspectives. Curr. Opin. Cell Biol. *40*, 1–7.
19. VanGompel, M.J., Nguyen, K.C., Hall, D.H., Dauer, W.T., and Rose, L.S. (2015). A novel function for the *Caenorhabditis elegans* torsin OOC-5 in nucleoporin localization and nuclear import. Mol. Biol. Cell *26*, 1752–1763.
20. Maric, M., Haugo, A.C., Dauer, W., Johnson, D., and Roller, R.J. (2014). Nuclear envelope breakdown induced by herpes simplex virus type 1 involves the activity of viral fusion proteins. Virology *460–461*, 128–137.
21. Jokhi, V., Ashley, J., Nunnari, J., Noma, A., Ito, N., Wakabayashi-Ito, N., Moore, M.J., and Budnik, V. (2013). Torsin mediates primary envelopment of large ribonucleoprotein granules at the nuclear envelope. Cell Rep. *3*, 988–995.
22. György, B., Cruz, L., Yellen, D., Aufiero, M., Alland, I., Zhang, X., Ericsson, M., Fraefel, C., Li, Y.C., Takeda, S., et al. (2018). Mutant torsinA in the heterozygous DYT1 state compromises HSV propagation in infected neurons and fibroblasts. Sci. Rep. *8*, 2324.
23. Ozelius, L.J., Page, C.E., Klein, C., Hewett, J.W., Mineta, M., Leung, J., Shalish, C., Bressman, S.B., de Leon, D., Brin, M.F., et al. (1999). The TOR1A (DYT1) gene family and its role in early onset torsion dystonia. Genomics *62*, 377–384.
24. Breakefield, X.O., Kamm, C., and Hanson, P.I. (2001). TorsinA: movement at many levels. Neuron *31*, 9–12.
25. Vander Heyden, A.B., Naismith, T.V., Snapp, E.L., Hodzic, D., and Hanson, P.I. (2009). LULL1 retargets TorsinA to the nuclear envelope revealing an activity that is impaired by the *DYT1* dystonia mutation. Mol. Biol. Cell *20*, 2661–2672.
26. Brown, R.S., Zhao, C., Chase, A.R., Wang, J., and Schlieker, C. (2014). The mechanism of Torsin ATPase activation. Proc. Natl. Acad. Sci. USA *111*, E4822–E4831.
27. Chase, A.R., Laudermilch, E., Wang, J., Shigematsu, H., Yokoyama, T., and Schlieker, C. (2017). Dynamic functional assembly of the Torsin AAA+ ATPase and its modulation by LAP1. Mol. Biol. Cell *28*, 2765–2772.
28. Zhao, C., Brown, R.S., Chase, A.R., Eisele, M.R., and Schlieker, C. (2013). Regulation of Torsin ATPases by LAP1 and LULL1. Proc. Natl. Acad. Sci. USA *110*, E1545–E1554.
29. Giles, L.M., Chen, J., Li, L., and Chin, L.S. (2008). Dystonia-associated mutations cause premature degradation of torsinA protein and cell-type-specific mislocalization to the nuclear envelope. Hum. Mol. Genet. *17*, 2712–2722.
30. Kock, N., Allchorne, A.J., Sena-Esteves, M., Woolf, C.J., and Breakefield, X.O. (2006). RNAi blocks DYT1 mutant torsinA inclusions in neurons. Neurosci. Lett. *395*, 201–205.
31. Heidenreich, M., and Zhang, F. (2016). Applications of CRISPR-Cas systems in neuroscience. Nat. Rev. Neurosci. *17*, 36–44.
32. Kleinstiver, B.P., Pattanayak, V., Prew, M.S., Tsai, S.Q., Nguyen, N.T., Zheng, Z., and Joung, J.K. (2016). High-fidelity CRISPR-Cas9 nucleases with no detectable genome-wide off-target effects. Nature *529*, 490–495.
33. György, B., Meijer, E.J., Ivanchenko, M.V., Tenneson, K., Emond, F., Hanlon, K.S., Indzhykulian, A.A., Volak, A., Karavitaki, K.D., Tamvakologos, P.I., et al. (2018). Gene transfer with AAV9-PHP.B rescues hearing in a mouse model of Usher syndrome 3A and transduces hair cells in a non-human primate. Mol. Ther. Methods Clin. Dev. *13*, 1–13.
34. György, B., Nist-Lund, C., Pan, B., Asai, Y., Karavitaki, K.D., Kleinstiver, B.P., Garcia, S.P., Zaborowski, M.P., Solanes, P., Spataro, S., et al. (2019). Allele-specific gene editing prevents deafness in a model of dominant progressive hearing loss. Nat. Med. *25*, 1123–1130.
35. Hanlon, K.S., Kleinstiver, B.P., Garcia, S.P., Zaborowski, M.P., Volak, A., Spirig, S.E., Muller, A., Sousa, A.A., Tsai, S.Q., Bengtsson, N.E., et al. (2019). High levels of AAV vector integration into CRISPR-induced DNA breaks. Nat. Commun. *10*, 4439.
36. Clement, K., Rees, H., Canver, M.C., Gehrke, J.M., Farouni, R., Hsu, J.Y., Cole, M.A., Liu, D.R., Joung, J.K., Bauer, D.E., and Pinello, L. (2019). CRISPResso2 provides accurate and rapid genome editing sequence analysis. Nat. Biotechnol. *37*, 224–226.
37. Kleinstiver, B.P., Prew, M.S., Tsai, S.Q., Topkar, V.V., Nguyen, N.T., Zheng, Z., Gonzales, A.P., Li, Z., Peterson, R.T., Yeh, J.R., et al. (2015). Engineered CRISPR-Cas9 nucleases with altered PAM specificities. Nature *523*, 481–485.
38. Hewett, J., Gonzalez-Agosti, C., Slater, D., Ziefer, P., Li, S., Bergeron, D., Jacoby, D.J., Ozelius, L.J., Ramesh, V., and Breakefield, X.O. (2000). Mutant torsinA, responsible for early-onset torsion dystonia, forms membrane inclusions in cultured neural cells. Hum. Mol. Genet. *9*, 1403–1413.
39. Kustedjo, K., Bracey, M.H., and Cravatt, B.F. (2000). Torsin A and its torsion dystonia-associated mutant forms are lumenal glycoproteins that exhibit distinct subcellular localizations. J. Biol. Chem. *275*, 27933–27939.
40. Turner, E.M., Brown, R.S., Laudermilch, E., Tsai, P.L., and Schlieker, C. (2015). The torsin activator LULL1 is required for efficient growth of herpes simplex virus 1. J. Virol. *89*, 8444–8452.
41. Gonzalez-Alegre, P., Miller, V.M., Davidson, B.L., and Paulson, H.L. (2003). Toward therapy for DYT1 dystonia: allele-specific silencing of mutant TorsinA. Ann. Neurol. *53*, 781–787.

42. Hewett, J.W., Nery, F.C., Niland, B., Ge, P., Tan, P., Hadwiger, P., Tannous, B.A., Sah, D.W., and Breakefield, X.O. (2008). siRNA knock-down of mutant torsinA restores processing through secretory pathway in DYT1 dystonia cells. Hum. Mol. Genet. *17*, 1436–1445.

43. Dang, M.T., Yokoi, F., Pence, M.A., and Li, Y. (2006). Motor deficits and hyperactivity in *Dyt1* knockdown mice. Neurosci. Res. *56*, 470–474.

44. Kariminejad, A., Dahl-Halvarsson, M., Ravenscroft, G., Afroozan, F., Keshavarz, E., Goullée, H., Davis, M.R., Faraji Zonooz, M., Najmabadi, H., Laing, N.G., and Tajsharghi, H. (2017). *TOR1A* variants cause a severe arthrogryposis with developmental delay, strabismus and tremor. Brain *140*, 2851–2859.

45. Isik, E., Aykut, A., Atik, T., Cogulu, O., and Ozkinay, F. (2019). Biallelic *TOR1A* mutations cause severe arthrogryposis: A case requiring reverse phenotyping. Eur. J. Med. Genet. *62*, 103544.

46. Reichert, S.C., Gonzalez-Alegre, P., and Scharer, G.H. (2017). Biallelic *TOR1A* variants in an infant with severe arthrogryposis. Neurol. Genet. *3*, e154.

47. Karczewski, K.J., Francioli, L.C., Tiao, G., Cummings, B.B., Alföldi, J., Wang, Q., Solomonson, M., Watts, N.A., Rhodes, D., Singer-Berk, M., et al. (2019). Variation across 141,456 human exomes and genomes reveals the spectrum of loss-of-function intolerance across human protein-coding genes. bioRxiv *28*, https://doi.org/10.1101/531210.

48. Pickar-Oliver, A., and Gersbach, C.A. (2019). The next generation of CRISPR-Cas technologies and applications. Nat. Rev. Mol. Cell Biol. *20*, 490–507.

49. Rees, H.A., Komor, A.C., Yeh, W.H., Caetano-Lopes, J., Warman, M., Edge, A.S.B., and Liu, D.R. (2017). Improving the DNA specificity and applicability of base editing through protein engineering and protein delivery. Nat. Commun. *8*, 15790.

50. Yeh, W.H., Chiang, H., Rees, H.A., Edge, A.S.B., and Liu, D.R. (2018). In vivo base editing of post-mitotic sensory cells. Nat. Commun. *9*, 2184.

51. Anzalone, A.V., Randolph, P.B., Davis, J.R., Sousa, A.A., Koblan, L.W., Levy, J.M., Chen, P.J., Wilson, C., Newby, G.A., Raguram, A., and Liu, D.R. (2019). Search-and-replace genome editing without double-strand breaks or donor DNA. Nature *576*, 149–157.

52. Maltese, M., Stanic, J., Tassone, A., Sciamanna, G., Ponterio, G., Vanni, V., Martella, G., Imbriani, P., Bonsi, P., Mercuri, N.B., et al. (2018). Early structural and functional plasticity alterations in a susceptibility period of DYT1 dystonia mouse striatum. eLife *7*, e33331.

53. Scarduzio, M., Zimmerman, C.N., Jaunarajs, K.L., Wang, Q., Standaert, D.G., and McMahon, L.L. (2017). Strength of cholinergic tone dictates the polarity of dopamine D2 receptor modulation of striatal cholinergic interneuron excitability in DYT1 dystonia. Exp. Neurol. *295*, 162–175.

54. Breakefield, X.O., Blood, A.J., Li, Y., Hallett, M., Hanson, P.I., and Standaert, D.G. (2008). The pathophysiological basis of dystonias. Nat. Rev. Neurosci. *9*, 222–234.

55. Hudry, E., and Vandenberghe, L.H. (2019). Therapeutic AAV gene transfer to the nervous system: a clinical reality. Neuron *101*, 839–862.

56. Afgan, E., Baker, D., Batut, B., van den Beek, M., Bouvier, D., Cech, M., Chilton, J., Clements, D., Coraor, N., Grüning, B.A., et al. (2018). The Galaxy platform for accessible, reproducible and collaborative biomedical analyses: 2018 update. Nucleic Acids Res. *46* (W1), W537–W544.

57. Robinson, J.T., Thorvaldsdóttir, H., Winckler, W., Guttman, M., Lander, E.S., Getz, G., and Mesirov, J.P. (2011). Integrative genomics viewer. Nat. Biotechnol. *29*, 24–26.

58. Baker, N.A., Sept, D., Joseph, S., Holst, M.J., and McCammon, J.A. (2001). Electrostatics of nanosystems: application to microtubules and the ribosome. Proc. Natl. Acad. Sci. USA *98*, 10037–10041.

59. Hornak, V., Abel, R., Okur, A., Strockbine, B., Roitberg, A., and Simmerling, C. (2006). Comparison of multiple Amber force fields and development of improved protein backbone parameters. Proteins *65*, 712–725.

60. Van Der Spoel, D., Lindahl, E., Hess, B., Groenhof, G., Mark, A.E., and Berendsen, H.J. (2005). GROMACS: fast, flexible, and free. J. Comput. Chem. *26*, 1701–1718.

61. Bussi, G., Donadio, D., and Parrinello, M. (2007). Canonical sampling through velocity rescaling. J. Chem. Phys. *126*, 014101.

62. Berendsen, H.J., Postma, J.V., van Gunsteren, W.F., DiNola, A.R., and Haak, J.R. (1984). Molecular dynamics with coupling to an external bath. J. Chem. Phys. *81*, 3684–3690.

63. Hess, B., Bekker, H., Berendsen, H.J.C., and Fraaije, J.G. (1997). LINCS: a linear constraint solver for molecular simulations. J. Comput. Chem. *18*, 1463–1472.

64. Jorgensen, W.L., Chandrasekhar, J., Madura, J.D., Impey, R.W., and Klein, M.L. (1983). Comparison of simple potential functions for simulating liquid water. J. Chem. Phys. *79*, 926–935.

65. de Oliveira, A.P., Glauser, D.L., Laimbacher, A.S., Strasser, R., Schraner, E.M., Wild, P., Ziegler, U., Breakefield, X.O., Ackermann, M., and Fraefel, C. (2008). Live visualization of herpes simplex virus type 1 compartment dynamics. J. Virol. *82*, 4974–4990.